Journal of Metals, Materials and Minerals, 37(1), e2719, 2027

Synergistic multifunctionality in $SrMnO_3$-ZrO_2 composite: Unravelling the dielectric relaxation and enhanced visible-light photocatalytic degradation of ciprofloxacin

Kirttimayee MOHANTA[1], Swayam Aryam BEHERA[1], Aniket PANDA[1], Raj MOHANTY[1], Asima SUBHADARSHINI[2], Binita NANDA[1], and P.Ganga Raju ACHARY[1,*]

[1] *Department of Chemistry, Siksha 'O' Anusandhan (Deemed to be University), Bhubaneswar-751030, India*
[2] *Department of Environmental Science, Siksha 'O' Anusandhan, (Deemed to be University), Bhubaneswar-751030, India*

***Corresponding author e-mail**: pgrachary@soa.ac.in

Received date:
14 April 2026
Revised date:
10 May 2026
Accepted date:
31 May 2026

Keywords:
Dielectric;
Impedance;
Photocatalysis;
Photo-oxidation;
Ciprofloxacin

Abstract

Zirconium modified strontium manganite composite is synthesized using an economically solid-state method. Orthorhombic symmetry is confirmed by structural analysis using X-ray diffraction (XRD) and the SEM analysis reveals the uniform dispersion of elements, chemical composition including morphology. The characteristic stretching and bending modes of the Sr–Mn–O and O–Mn–O bonds in the octahedral SrO_6 unit were identified by Fourier-transform infrared (FTIR) spectroscopy. Optical bandgap values, measured by UV-visible diffuse reflectance spectroscopy (DRS), show a composition-dependent bandgap value of 2.57 eV for the 1:1 ratio. Electrical measurements indicate that the transport mechanism is dominated by a hopping-type charge transfer process. The SMOZr (1:1) composite shows enhanced photocatalytic activity with an efficiency of 88.3% degradation of ciprofloxacin (CIP) under visible light irradiation. The catalyst shows high stability and recyclability over four consecutive cycles. The kinetic studies establish the pseudo-first-order degradation of the pollutant, which highlights the robustness of this stable multifunctional perovskite material for environmental applications.

As we have taken different molar mixtures of both the pristine, it is difficult to get the Rietveld fitting of the composite. Here in Figure S1(a) and Figure S1(b) we have provided the separate fitting data of both the pristine which is possible to correlate with the composite structure. The Rietveld refinement of $SrMnO_3$ powders at room temperature is shown in Figure S1(a) which comprises of 2 phases; one of $SrMnO_3$ and other of $Sr(MnO_4)_2$ with mass percentages 71.26% and 28.84% respectively, with R_p value at 10.495%, R_{wp} value at 12.715%, R_{exp} value of 3.38% and with a sigma value (χ^2) of 3.76, which are good fitting parameters, indicate that the resulting samples are of high quality. On the other hand, for ZrO_2 powders at room temperature as shown in Figure S1(b) the R_p value is at 12.99%, R_{wp} value at 15.87%, R_{exp} value of 7.3% and with a sigma value (χ^2) of 2.17, which are good fitting parameters, indicating that the resulting samples are of high quality.

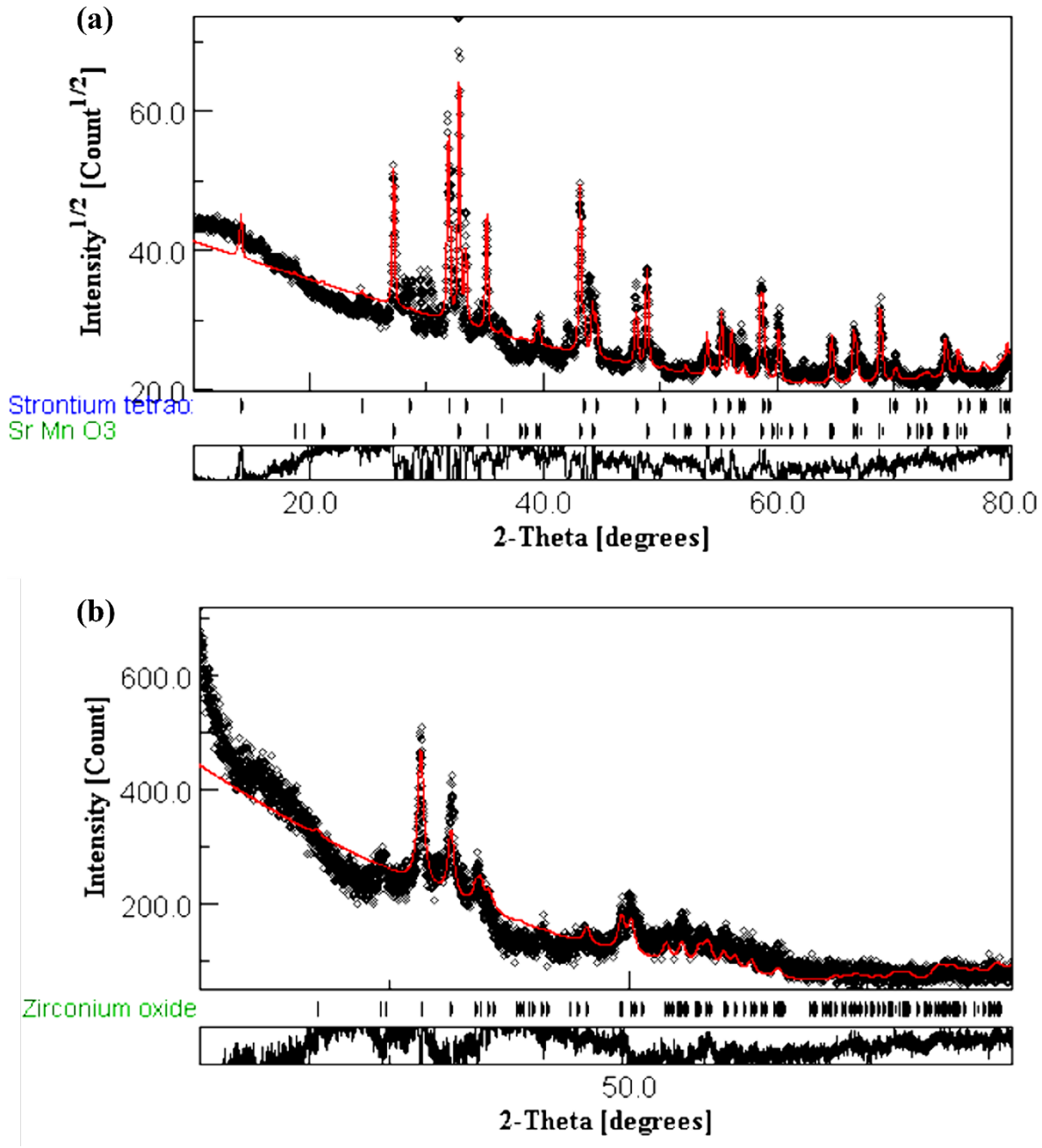

Figure S1. Rietveld refinement analysis of XRD pattern of (a) $SrMnO_3$ (b) ZrO_2

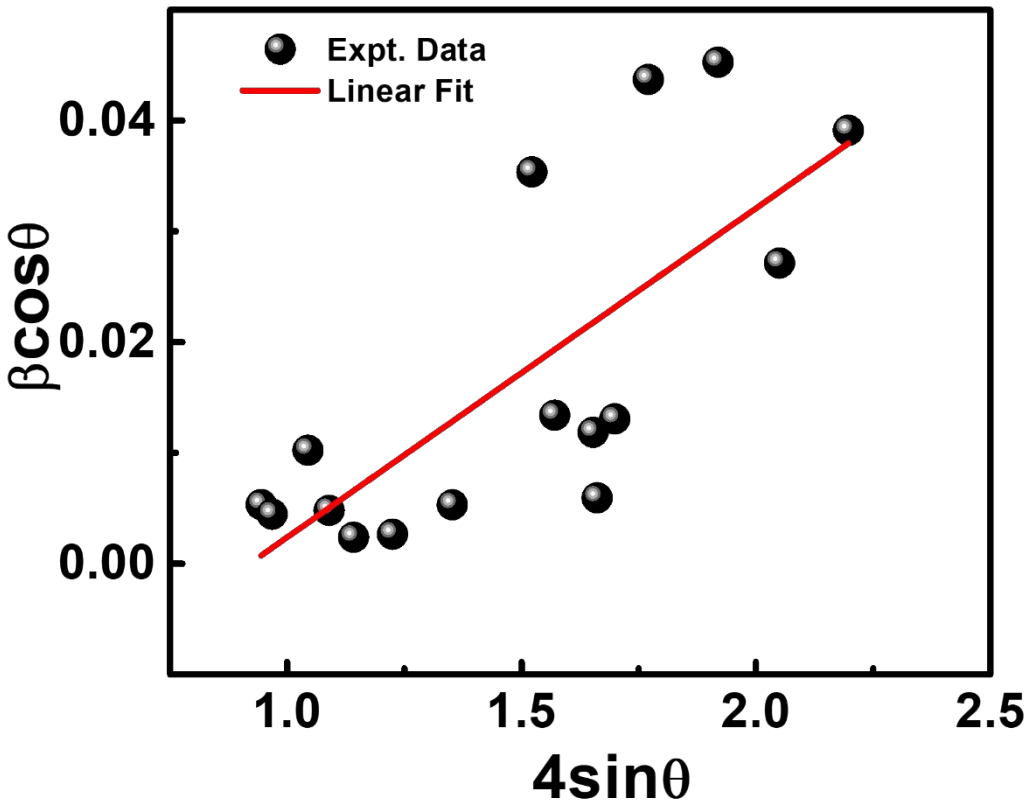

Figure S2. Williamson-Hall Plot of $SrMnO_3$:ZrO_2 composite.

The crystallite size and lattice strain were evaluated using the Williamson-Hall (W-H) method according to the equation:

$$\beta \cos\theta = \frac{k\lambda}{D} + 4\varepsilon \sin\theta$$

Where, D is the crystallite size and ε is the lattice strain. A linear fit of $\beta \cos\theta$ versus 4 $\sin\theta$ yielded a positive slope, indicating the presence of tensile micro strain within the crystal lattice. The observed scattering of data points around the fitted line suggests non-uniform strain distribution and lattice imperfections. The relatively large slope signifies that strain-induced broadening contributes significantly to the overall peak broadening. Such lattice distortions may originate from structural defects, dislocations, grain boundaries, and interfacial interactions within the composite material. The weak intercept obtained from the fit indicates that strain broadening dominates over crystallite-size broadening, making micro strain the principal factor affecting the diffraction peak widths which is shown in Figure S2. From the graph, we have found the intercept to be 0.0273 from which using the equation we found the crystallite size to be around 5.02 nm. Again, from the graph, the slope of the graph is found to be 0.0297 which is also the lattice strain of the nano composite. The small crystallite size confirms the nanocrystalline nature of the synthesized material, while the relatively high positive lattice strain indicates the presence of significant lattice distortions and structural defects within the crystal framework. Such strain may arise from grain boundaries, dislocations, interfacial interactions, and the incorporation of secondary phases or filler particles. The results suggest that strain-induced broadening contributes substantially to the diffraction peak broadening, indicating that micro strain plays a dominant role in determining the structural characteristics of the material. The combination of nanoscale crystallites and appreciable lattice strain is expected to enhance the surface reactivity and defect density, which can be beneficial for applications involving charge transfer, photocatalysis, sensing, and energy harvesting.